Optical properties and temperature dependence of the interband transitions of cubic and hexagonal GaN

S. Logothetidis and J. Petalas
Department of Physics, Solid State Section, Aristotle University of Thessaloniki, GR 54006 Thessaloniki, Greece

M. Cardona
Max-Planck-Institut für Festkörperforschung, Heisenbergstrasse 1, D-70569 Stuttgart, Germany

T. D. Moustakas
Department of Electrical, Computer and Systems Engineering, Boston University, Boston, Massachusetts 02215
(Received 27 June 1994)

The optical properties of cubic and hexagonal GaN thin films, grown by electron-cyclotron resonance microwave plasma-assisted molecular-beam epitaxy on silicon and sapphire substrates, respectively, have been studied at photon energies up to 25 eV with conventional and synchrotron-radiation spectroscopic ellipsometry. The fundamental gaps of the two polytypes are located at different energies, namely at 3.25 and 3.43 eV for cubic and hexagonal GaN. Analysis of the dielectric function of the two phases in the region 4.5–9.5 eV with appropriate models yields the energy location and broadening of the observed critical points. These critical points are assigned to specific points in the zinc-blende and wurtzite Brillouin zones, respectively, making use of the latest published band-structure studies and a comparison is made between the corresponding results for GaN, GaAs, and GaP. Measurements in the temperature range from 80 to 650 K provide the temperature dependence of these parameters. The features observed in the reflectivity spectra of hexagonal GaN are discussed in relation to other works. Kramers-Kronig analysis of the reflectivity between 0 and 33 eV of the hexagonal polytype verifies the existence of a broad feature centered at 14 eV. Finally, average properties, such as the effective ir dielectric constant and the effective number of valence electrons per atom are calculated for the two polytypes and compared to GaAs and GaP.

I. INTRODUCTION

The development in the past decade of light-emitting diodes and semiconductor lasers operating in the red to green spectral region and the aim to realize full-color display systems has prompted the search for devices operating in the blue/ultraviolet (UV) energy range. GaN is a promising candidate for the fabrication of such devices, since it possesses a direct gap in the near UV (around 3.4 eV), is resistant to radiation damage, and can form solid solutions with InN and AlN, which permits the tailoring of its optical and electrical behavior.[1] The latest applications of GaN in optical and microelectronics structures involve device-quality contacts;[2] UV photoconductors;[3] *p-n* junctions and diodes;[4–6] InGaN/GaN and AlGaN/GaN double-heterostructure UV/blue LED's;[4,7] multilayers[8] and superlattices;[9] metal-insulator-semiconductor[5,10] and SIS (Ref. 11) structures; and high-electron-mobility[12] and metal-semiconductor-field-effect[13] transistors. These devices are all based on the widely studied hexagonal GaN polytype, but recently rapid advances have been achieved in depositing high-quality GaN in the cubic form.[14–17] Magnetic-resonance phenomena are also attracting considerable attention on both GaN polytypes.[18,19]

GaN forms bonds considerably shorter ($\approx$20%) than most semiconductors, has large ionicity, and exhibits high hardness and thermal conductivity. Such physical and structural properties of GaN can be considered extreme in comparison with the majority of III-V and II-VI materials and, therefore, the material offers a very interesting test case for the various theoretical prediction schemes of the properties and behavior of III-V compounds. Until the mid 1980's, hexagonal (wurtzitelike) GaN (α-GaN) was the only known polytype and a number of pioneering theoretical works focused on its electronic properties.[20–23] In the past decade, the discovery of various potential applications revived the interest in the material.[24–32] On the other hand, the deposition of the highly promising cubic phase was accomplished only in recent years, and thus, theoretical works on its electronic band structure are just beginning to appear.[28–31]

The deposition of α-GaN has been successful on various substrates, such as Si (111),[33] sapphire at various orientations [mainly (0001)], but also (01$\underline{1}$2),[34] (11$\underline{2}$0),[33] and (1$\underline{1}$02),[23] GaAs(111),[35] as well as on 6H-SiC(0001),[36–38] with which the lattice and thermal expansion mismatch is very low. An AlN (Refs. 12, 39–41) or GaN (Refs. 7, 33, 41) buffer layer is reported to improve the surface morphology and electrical properties of the material. α-GaN is prepared mainly by metal-organic vapor-phase epitaxy and metal-organic chemical-vapor deposition, as well as gas-source[42] (GS) and electron-cyclotron resonance[33] (ECR) molecular-beam epitaxy (MBE). Less common growth techniques include atomic-layer epitaxy[38] at low temperatures, hydride

0163-1829/94/50(24)/18017(13)/$06.00

vapor-phase epitaxy[6] and high gas-pressure growth.[43]

Cubic (zinc-blende) GaN (β-GaN) is though to accept n- and p-type dopants more efficiently than its wurtzite counterpart, but was not until recently successfully produced, due to the lack of suitable substrates. The material can now be epitaxially grown on GaAs(001) (Ref. 35) and (100),[14,44] Si(100) (Refs. 15 and 33) and (001),[16] and β-SiC(100) (Ref. 17) with which the lattice mismatch is lower than 4%.

The potential applications of the material in optoelectronics render imperative the detailed knowledge of its optical response. The electronic and optical properties of GaN above the fundamental absorption edge have not yet been widely investigated and the reflectivity peaks observed in the literature are not undisputedly assigned to specific points of the corresponding Brillouin zone. Little work has been done on the wurtzite polytype,[21–23,45–49] whereas on its zinc-blende counterpart, which was successfully grown only recently, no experimental data have been reported up to now concerning the higher interband transitions and their origin. In an aim to fulfill the above gap, we present a study of the optical properties of the cubic and hexagonal polytypes of GaN in the vacuum-ultraviolet region by means of spectroscopic ellipsometry performed with synchrotron radiation and compare the experimental results with theoretical predictions, in order to assign the observed spectral features to electronic transitions at specific points of the Brillouin zone (BZ).

We present experimental details of this work in Sec. II. A brief description of the theoretical model used in the analysis is given in Sec. III and results are given in Sec. IV. The discussion, Sec. V, focused on the nature of the observed gaps (Sec. V A), their temperature dependence (Sec. V B), the reflectivity features of α-GaN in the energy region 4.5–9.5 eV (Sec. V C), and the origin of the feature around 14 eV reported in the literature for α-GaN (Sec. V D), whereas average properties via the application of sum rules are estimated for GaN in Sec. V E. The conclusions of this work are summarized in Sec. VI.

II. EXPERIMENT

The GaN films have been grown with the electron-cyclotron resonance microwave-plasma-assisted MBE (ECR-MBE). In this method, the film growth proceeds by the reaction of Ga vapor with ECR-activated molecular nitrogen and takes place mainly at low temperatures and ultrahigh vacuum conditions (base pressure 10^{-11} Torr). Growth on Si(100) and (001) leads to the formation of single-crystalline cubic GaN films having the zinc-blende structure,[33] whereas growth on Si(111) results in the wurtzite (hexagonal) structure, reported to have a large concentration of (111) stacking faults and, therefore, a significant cubic component.[33] On the other hand, growth on sapphire substrates leads to the formation of wurtzite single-crystalline GaN structures.[33] The structure and morphology of the β- and α-GaN samples was examined by reflection high-energy electron diffraction, x-ray diffraction, and transmission- and scanning-electron-microscopy techniques[33,50] and their thickness was 0.7 and 4.0 μm, respectively.

The optical properties of GaN are studied with spectroscopic ellipsometry, a nondestructive technique that measures directly the complex dielectric function $\varepsilon(\omega)$ $[=\varepsilon_1(\omega)+i\varepsilon_2(\omega)]$ of materials.[51] This function yields a complete picture of the linear optical response and provides valuable information on the electronic structure, since its imaginary part $\varepsilon_2(\omega)$ is directly associated to the joint density of states for interband transitions.[52] The GaN thin films were measured in the energy region 1.5–6.3 eV at the rotating analyzer ellipsometer of the University of Thessaloniki using a Xe lamp as the light source and in the energy regions 4.5–9.5 eV and 14–25 eV using synchrotron radiation from the storage ring (BESSY), Berlin, as the light source.[53,54] The angle of incidence of the light beam was 67.5° in all measurements up to 10 eV and 45° in the 14–25-eV region. In the intermediate energy region (9.5–14 eV), the nominally monochromatic radiation is plagued by contamination with second-order radiation, which distorts the line shape and modifies the absolute values of the measured spectra. In order to investigate the dependence of the optical properties on temperature, measurements were performed in the temperature range 80–650 K. The α- and β-GaN specimens were cleaned before placing them in the UHV chamber by a four-stage procedure, which is reported to remove organic contaminants from the samples surface, namely successive heating at 50 °C for 10 min in trichoroethylene, acetone, and methanol and finally rinsing in deionized water.

III. MODELING OF THE DIELECTRIC-FUNCTION SPECTRA

The observed features in the optical spectra of crystalline materials correspond to interband electronic transitions occurring at specific points in the Brillouin zone of the crystal, the so-called critical points (CP's), where the transition probability becomes maximum. The knowledge of CP's is essential for a thorough understanding of the dielectric response and a consistent prediction of its optical and electrical properties. In an aim to analyze the measured $\varepsilon(\omega)$ spectra, we employ the model suggested in Ref. 52, which considers $\varepsilon_2(\omega)$ as a sum of contributions from all direct gaps (i.e., from all CP's) and describes the dielectric function for the case of one CP with the following relation:

$$\varepsilon(\omega)=C-Ae^{i\varphi}(\omega-E+i\Gamma)^n \ . \tag{1}$$

The parameters E and Γ designate the energy location and broadening of the CP, respectively, whereas A is a measure of the transition strength. The phase factor φ and the exponent n are related to the shape of the valence and conduction bands and the electron effective mass in the neighborhood of the CP.[55] We analyze the first- and second-derivative spectra of the dielectric function according to Eq. (1), in order to enhance the spectral features and analyze them by fitting them to the corresponding derivatives of Eq. (1).

IV. RESULTS

Since hexagonal materials are optically anisotropic, the wurtzite GaN samples were first of all measured at various orientations, i.e., by rotating the specimens around the axis perpendicular to their surface. The obtained dielectric-function spectra showed no noticeable differences, a fact that implies that the optical axis (i.e., the hexagonal c axis) of the films is perpendicular to the substrate plane. Therefore, the films exhibit no surface anisotropy, in agreement with x-ray measurements,[50] and the measured dielectric response corresponds to $E \perp c$, E being the electric field of the incident light beam. A complete description of the effect of optical anisotropy on the dielectric function is reported for wurtzite CdSe in Ref. 56.

In Fig. 1 we present the dielectric-function spectra of cubic (β-) and hexagonal (α-) GaN thin films grown on silicon and sapphire substrates, respectively, in the energy region 3–10 eV and at room temperature (RT). The arrows designate the location of structures in the experimental spectra. At energies below 3 eV, the GaN films are transparent and, thus, the spectra are dominated by interference fringes originating from the multiple reflection of the incident light beam at the film/substrate interface. From this figure it is obvious that the optical response of the two polytypes is rather different. Such behavior is not unusual and has also been reported for the case of cubic and hexagonal CdS.[57] One can note the considerable differences in the energy position and number of occurring peaks, as well as the absolute values of $\varepsilon(\omega)$. The first structures above the fundamental gap almost coincide in energy for the two GaN polytypes, with E_{1H} being somewhat lower in energy than E_{1C}, in a manner identical to what is observed in CdS.[56]

As seen from Fig. 1, the fundamental absorption of the cubic and hexagonal polytypes is located at different energies. A detailed analysis for the extraction of the optical gap taking into account interference effects is presented in Ref. 50 and yielded the values 3.25 and 3.43 eV, respectively. In Figs. 2 and 3, we present the dielectric-function spectra of cubic and hexagonal GaN at various temperatures in the energy region above the fundamental gap, i.e., 5–9.5 eV. As expected, the spectral features become sharper with decreasing temperature and shift by ≈ 0.2 eV between 83 and 570 K, whereas the absolute values of the dielectric function increase.

For the case of β-GaN, the $\varepsilon(\omega)$ spectrum is dominated by one major structure that consists of two adjacent peaks, at around 7.0 and 7.6 eV, denoted E_{1C} and E_{2C} in Fig. 1. The main peak was analyzed by fitting the first-derivative ($d\varepsilon/d\omega$) spectra to the derivative of Eq. (1). Since the material exhibits broad structures, their second-derivative spectra were somewhat noisy and difficult to fit. The best fits succeeded assuming two-dimensional (2D) CP's and revealed the existence of two nearly energy-degenerate CP's located at 6.95 (4) and 7.58 (1) eV (at RT), with respective broadenings 274 (60) and 90 (10) meV. Furthermore, a weak shallow shoulder, which is often difficult to detect, appears in the dielectric-function spectra at energies around 8.8 eV.

Figure 3 shows that the $\varepsilon(\omega)$ spectrum of wurtzite GaN is rich in features in the UV region. Three structures appear in $\varepsilon_2(\omega)$ at 7.0, 7.9, and 9.0 eV; they are denoted E_{1H}, E_{2H}, and E_{3H}, respectively, (refer also to Fig. 1). The assumption of 2D line shapes gave the best fits and thus the analysis of the first- and second-derivative ($d^2\varepsilon/d\omega^2$) dielectric-function spectra yielded the same results and revealed the existence of at least two structures in the energy region 6–8.5 eV, located at 6.98 (6) and 7.93 (18) eV (RT), with respective broadenings 204 (50) and 259 (70) meV (second-derivative results). The third structure (E_{3H}) was difficult to analyze at high temperatures and was estimated to lie at 8.71 (11) eV.

We have indications of an additional weak structure situated between E_{1H} and E_{2H}, higher than E_{1H} by around 200 meV, which was difficult to detect even in the derivative experimental spectra and could be only analyzed at temperatures below 150 K. A typical spectrum

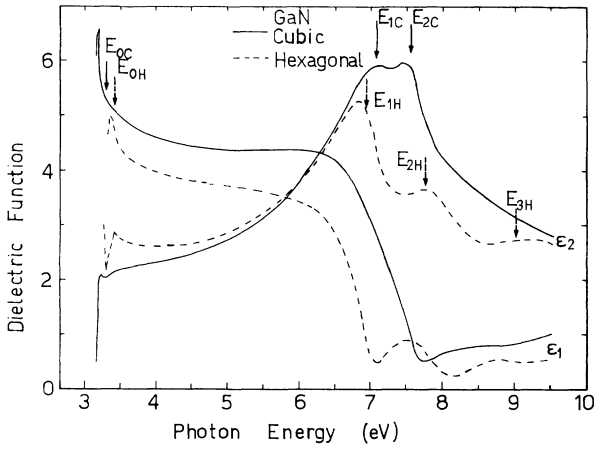

FIG. 1. The real (ε_1) and imaginary (ε_2) part of the dielectric function of cubic and hexagonal GaN (solid and dashed lines, respectively) in the energy region 3–10 eV. The arrows indicate the location of interband transitions, as assigned to the observed structures.

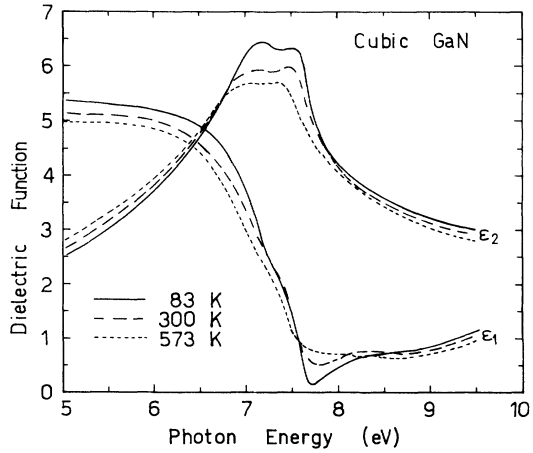

FIG. 2. The real (ε_1) and imaginary (ε_2) part of the dielectric function of cubic GaN (β-GaN) in the energy region 5–10 eV at various temperatures.

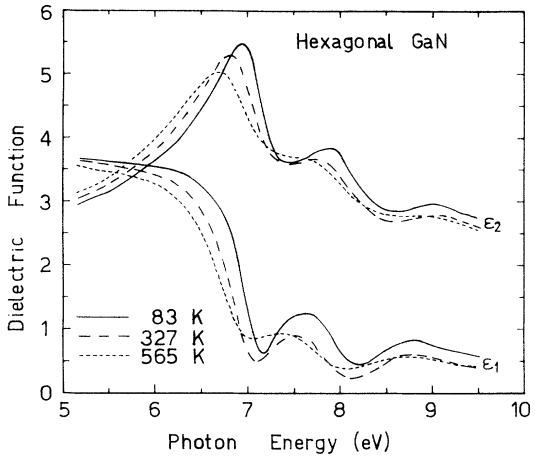

FIG. 3. The real (ε_1) and imaginary (ε_2) part of the dielectric function of hexagonal GaN (α-GaN) in the energy region 5–10 eV at various temperatures.

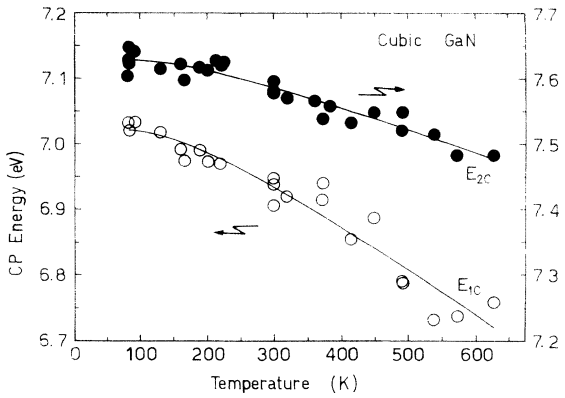

FIG. 5. Temperature dependence of the energy position of the E_1 and E_2 critical points of cubic GaN (open and solid circles). The energy values shown refer to analysis of the first-derivative dielectric-function spectra. The solid lines represent fits to the data with Eq. (3).

of the second derivative of the experimental dielectric function at low temperatures (83 K) is presented in Fig. 4 (open and solid circles). The dashed and solid lines in this figure designate fits to the experimental points with the model given in Eq. (1) and assuming two and three CP's, respectively, in the energy region between 6 and 8.5 eV. The consideration of this additional structure in the fitting ameliorates fairly the matching between experiment and fit. Yet, this is somewhat expected, since in this way four additional fit parameters are introduced.

The energy shift with temperature of the CP energies for cubic and hexagonal GaN are presented in Figs. 5 and 6, respectively. The points shown correspond to first- (β-GaN) and second-derivative analysis (α-GaN) of the dielectric function and were fitted with the empirical Varshni expression,[58]

$$E(T)=E_0-\frac{aT^2}{T+\beta}\ , \tag{2}$$

as well as considering an average Bose-Einstein statistical factor (solid lines in Figs. 5 and 6), which assumes crystal phonons to have mean energy Ω, an approximation that leads to $\Omega=k_B\Theta$,

$$E(T)=E_B-a_B\left[1+\frac{2}{e^{\Theta/T}-1}\right]\ . \tag{3}$$

The temperature dependence of the broadening parameter Γ of the E_1 and E_2 CP's of cubic and hexagonal GaN is presented in Figs. 7 and 8, respectively. The points shown were obtained from fits to the first (β-GaN) and second derivative (α-GaN) of the experimental spec-

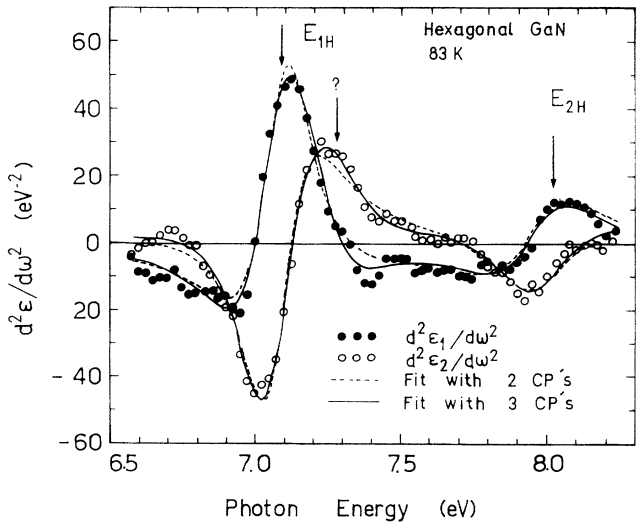

FIG. 4. Fits to the second derivative of the dielectric function of α-GaN around the E_{1H} and E_{2H} structures at 83 K, assuming the contribution of two (dashed lines) and three (solid lines) CP's to $\varepsilon(\omega)$. The data represent the experimental data for $d^2\varepsilon_1/d\omega^2$ and $d^2\varepsilon_2/d\omega^2$.

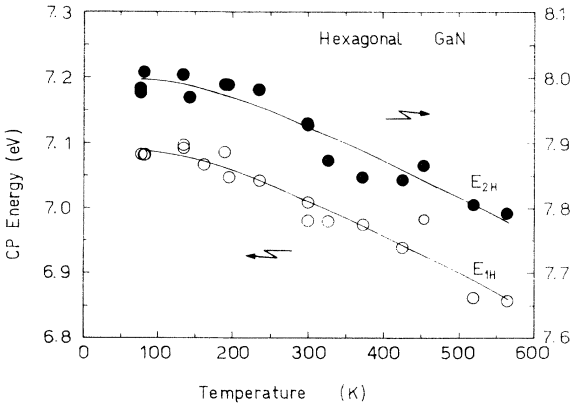

FIG. 6. Temperature dependence of the energy position of the E_1 and E_2 critical points of hexagonal GaN (open and solid circles). The energy values shown refer to analysis of the second-derivative dielectric-function spectra. The solid lines represent fits to the data with Eq. (3).

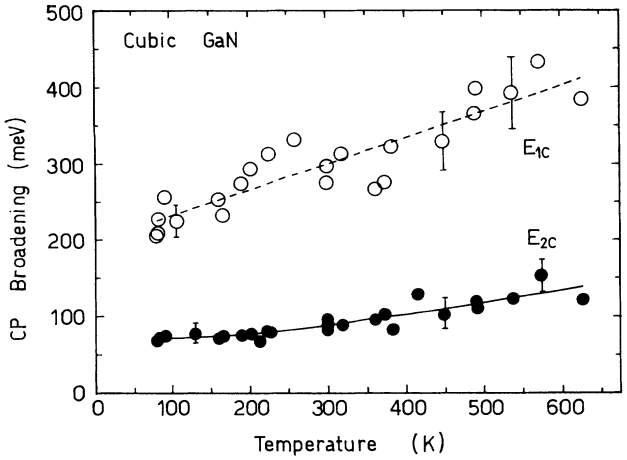

FIG. 7. Temperature dependence of the broadening parameter of the E_1 and E_2 critical points of cubic GaN (open and solid circles). The broadening values shown refer to analysis of the first-derivative dielectric-function spectra. The solid and dashed lines represent fits to the data with Eqs. (4) and (5), respectively.

tra. The solid lines in Figs. 7 and 8 correspond to fits of the data with the Bose-Einstein model, which for the case of phonon-induced lifetime broadenings takes the form[59]

$$\Gamma(T)=\Gamma_1+\Gamma_0\left[1+\frac{2}{e^{\Theta/T}-1}\right] . \quad (4)$$

The first term of this expression represents the broadening due to temperature-independent mechanisms (Auger processes, impurity and surface scattering, electron-electron interaction, inhomogeneous broadening), whereas the second is due to electron-phonon interaction. The dashed lines in Figs. 7 and 8 designate fits of the data assuming a linear relation of the form

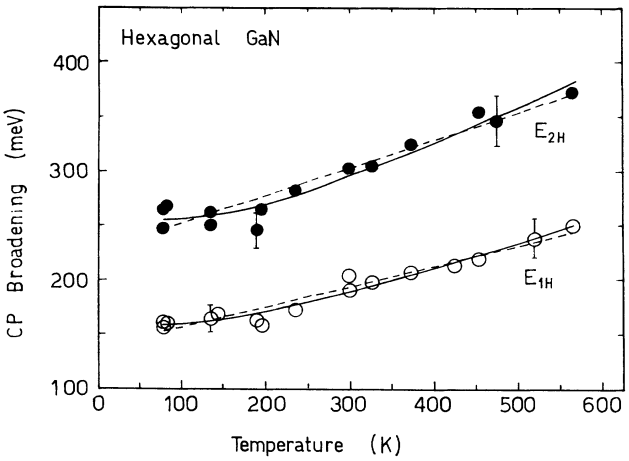

FIG. 8. Temperature dependence of the broadening parameter of the E_1 and E_2 critical points of hexagonal GaN (open and solid circles). The broadening values shown refer to analysis of the second-derivative dielectric-function spectra. The solid and dashed lines represent fits to the data with Eqs. (4) and (5), respectively.

$$\Gamma(T)=\Gamma_L+\gamma T . \quad (5)$$

The values of the best-fit parameters of Eqs. (2)–(5) used to describe the temperature dependence of the energy location and broadening of the CP's of cubic and hexagonal GaN in the region 5–8.5 eV are listed in Tables I and II, respectively. Due to the scatter of the experimental data, the estimated 95% error bars (numbers in parentheses in Tables I and II) are high. The temperature coefficients of β-GaN for temperatures up to and above 300 K are presented in Table III.

V. DISCUSSION

A. Origin of the critical points of cubic and hexagonal GaN

The fundamental absorption edge of β-GaN has been estimated by various authors[23,60] to lie around 3.4–3.5 eV and is accepted to correspond to an E_0 (Γ_6-Γ_1) transition at the center of the BZ. Its location is found to be at 3.25 eV, slightly lower than that of the wurtzite polytype (3.43 eV). The higher-energy spectra of the β-GaN (refer to Fig. 1) are dominated by a major structure in the region 6.8–8.0 eV consisting of two neighboring peaks, labeled E_{1C} and E_{2C} in Fig. 1 and located at around 7.0 and 7.6 eV at RT (refer also to Fig. 3), whereas no detectable structure is observed in the regions 5–6.8 and 8–9.5 eV. In order to investigate the nature of the observed peaks we refer to electronic structure studies in the literature. Among the published theoretical works, the most reliable band-structure data seem to be those of Miwa and Fukumoto[28] and Rubio *et al.*[31] The corresponding methods are first-principles pseudopotential calculations without local-density-approximation (LDA) adjustment and with (GW)-quasiparticle correction, respectively. The latter method does not suffer from the systematic error induced in the calculation of the conduction-band states by LDA and, therefore, can provide rather trustworthy data for the interband electronic excitations; however, in that work[31] the GW-corrected band-structure diagram is not presented.

Therefore, in order to give an impression of the band structure of zinc-blende GaN (β-GaN), we present in Fig. 9 the corresponding calculation performed by Miwa and Fukumoto.[28] This figure shows that the absolute value of the fundamental gap E_0 is underestimated and is found to occur low in energy, at about 2.7 eV. The corresponding theoretical results on the energy location of the electronic transitions up to 10 eV are compared with our experimental data in Table IV. Hence, Miwa and Fukumoto estimate the fundamental transitions at the L and X points to occur at 5.8 eV (X_5-X_1) and 6.0 eV (L_3-L_1), respectively, whereas Rubio *et al.*[31] seem to provide absolute values for these gaps that are in better agreement with experiment, i.e., 7.7 and 7.3 eV, respectively. The first direct gap at the K point (K_2-K_1) is reported to occur at nearby energies[30] and a values of 7.0 eV is estimated by Miwa and Fukomoto.

TABLE I. Values of the parameters obtained by fitting the temperature dependence of the energies of the E_1 and E_2 critical points of cubic and hexagonal GaN with Eqs. (2) and (3). The numbers in parentheses indicate the 95% confidence limits.

	CP	E_0 (eV)	α (10^{-4} eV/K)	β (K)	E_B (eV)	a_B (eV)	Θ (K)
GaN cubic	E_1	7.03 (3)	9.5 (3.8)	553 (460)	7.19 (15)	0.17 (10)	471 (320)
	E_2	7.63 (1)	4.6 (1.7)	500 (420)	7.72 (6)	0.09 (7)	479 (270)
GaN hexag.	E_1	7.10 (2)	8.9 (3.6)	621 (450)	7.23 (13)	0.14 (10)	461 (300)
	E_2	8.01 (3)	7.7 (3.5)	503 (360)	8.15 (17)	0.15 (12)	486 (400)

In group-IV elements and III-V compounds the second direct gap (usually labeled E_1) is attributed to transitions around the L point and/or along the Λ (Γ-L) direction. The third direct gap (designated E_2) is usually of more complex origin and assigned to more than one regions of the Brillouin zone (among them the X point) and, thus, is found to exhibit generally higher broadening parameters than E_1, a fact that is likely to result from the extended nature of the critical point or points and is often called "inhomogeneous broadening." The two gaps differ by more than 1.0 eV in energy in most of these materials and hence consist of well differentiated features in the optical spectra. In the case of β-GaN (refer to Fig. 2) and in accordance with the band-structure results, we believe that the gaps E_1 and E_2 lie closer in energy ($\approx$0.6 eV) than for most III-V materials, leading to the double structure between 6.8 and 8.0 eV. We, therefore, suggest that the features designated E_{1C} and E_{2C} in Fig. 1 correspond to the E_1 and E_2 gaps, respectively.

Apart from the Λ direction, the E_1 CP's of GaAs and GaP are attributed to a region along the ΓKL plane.[61-64] This should be considered also in the case of β-GaN, since the bands along the Λ line are found to be parallel over a wide wave-vector region towards the L point. A theoretical study would clarify this point, as well as a possible contribution from the K point. A comparison between the assignment of the E_1 and E_2 structures of β-GaN, and GaAs and GaP to specific regions in the Brillouin zone is shown in Table V.

The E_2 transition, in the case of GaAs and GaP, is a sum of several contributions, mainly from an extended region in the ΓXUL plane [denoted $E_2(P)$].[61,63] A contribution from the K point [$E_2(\Sigma)$] is also reported for GaAs,[61,63,64] whereas the Δ line (Γ-X) presents a high joint density of states in the case of GaP [$E_2(\Delta)$].[61,64] In the region around the X point, several transitions of generally small strength are reported to occur [$E_2(X)$],[61,62,64-66] although recent works do not support this argument for GaAs.[67,68] In the case of GaN the E_2 structure should be attributed to the X point of the BZ, whereas a possible contribution from the ΓXUL plane should not be excluded.

The values of the broadening parameter of the E_1 and E_2 transitions of GaAs,[65] GaP,[66] and GaN are shown in Table V. The analysis of the critical-points broadenings (refer to Fig. 7) of β-GaN yields that the E_1 CP exhibits broadening values significantly higher ($\approx$300 meV at RT) than the neighboring E_2 CP ($\approx$80 meV) and the E_1 CP's of GaAs and GaP. This might further support the argument that the E_1 CP is, unlike GaAs and GaP, a contribution from transitions over a broad wave-vector range (Fig. 9). On the other hand, reliable band-structure calculations with estimation of the band-to-band contributions to the dielectric function need to be made in order to determine the location of the E_1 structure, as well as investigate a possible contribution to E_2 from the ΓXUL plane.

From the above, it can be concluded that the experimentally observed broad structure in the region 6.8–8.0 eV is of complex origin and namely a superposition of the E_1 and E_2 gaps. The former is suggested to comprise of interband transitions that occur at nearby energies around 7.0 eV and take place at different points of the BZ (mainly along the Λ line and the L point) but could be associated with the K point, unless proved otherwise. The latter gap is, unlike other III-V materials, well defined at 7.6 eV and may correspond to excitations around the X point. Furthermore, the weak shoulder at 8.8 eV could be related to the E_1' gap of the material. The arrows in Fig. 9 designate the assignment of the E_1 and E_2 structures to specific interband transitions in the BZ of β-GaN.

The BZ of the wurtzite lattice involves more high-symmetry points than the zinc-blende one and, therefore,

TABLE II. Values of the parameters obtained by fitting the broadening of the E_1 and E_2 critical points of cubic and hexagonal GaN vs temperature according to Eqs. (4) and (5). The numbers in parentheses indicate the 95% confidence limits.

	CP	Γ (meV)	Γ_0 (meV)	Θ (K)	Γ_L (meV)	γ (meV/K)
GaN cubic	E_1				198 (24)	0.34 (7)
	E_2	27 (20)	44 (50)	522 (420)	56 (8)	0.12 (2)
GaN hexag.	E_1	100 (44)	59 (40)	467 (250)	138 (8)	0.19 (3)
	E_2	161 (90)	94 (90)	516 (340)	227 (14)	0.25 (4)

TABLE III. Temperature coefficients of the critical-point energies of the E_1 and E_2 CP's of the zinc-blende Ga-V compounds in the temperature regions up to 300 K and above 300 K (in 10^{-4} eV/K). The numbers in parentheses designate the 95% confidence limits.

CP	GaAs[a]	GaP[b]	GaN[c]
	Temperatures up to 300 K		
$-dE_1/dT$	5.2 (1)	4.3 (1)	4.5 (8)
$-dE_2/dT$	6.3 (4)	2.6 (6)	1.9 (8)
	Temperatures above 300 K		
$-dE_1/dT$	6.4	4.8	6.4 (9)
$-dE_2/dT$	6.5	3.6[d]	3.0 (6)

[a]Reference 65.
[b]Reference 66.
[c]This work.
[d]Mean value between the temperature coefficients of the $E_2(\Delta)$ and $E_2(P)$ CP's.

TABLE IV. Calculated energy values of the critical-point energies of the major structures observed in the $\varepsilon_2(\omega)$ up to 10 eV of β-GaN, according to the most reliable band-structure data found in the literature. The corresponding energies of the experimental dielectric-function structures are also noted.

		Energy (eV)		
Transition		Miwa and Fukumoto (FP-PSPT)[a]	Rubio *et al.* (FP-PSPT)[b]	This work (experiment)
E_0	Γ_{15}-Γ_1	2.7	3.1	3.25
E_1	L_3-L_1	6.0	7.3	7.0
	K_2-K_1	7.0		
E_2	X_5-X_1	5.8	7.7	7.6

[a]First-principles pseudopotential calculation without LDA adjustment, Ref. 28.
[b]First-principles pseudopotential calculation with GW-quasiparticle adjustment, Ref. 31.

hinders the undisputable assignment of experimental features to specific electronic transitions. Among the variety of published works, there exist converging results, which provide accurate determinations of the fundamental gap and yield reliable data concerning the higher energy gaps (Huang and Ching,[24] Gorczyca and Christensen,[25] and Xu and Ching[26]). The corresponding data are listed in Table VI. Even though the data of Xu and Ching yield slightly lower values for all gaps in comparison to the other two works, we believe that this is a systematic underestimation by a value of 0.3–0.5 eV for the gaps under study, which causes no change in the overall picture. On the other hand, Rubio *et al.*[31] seem to report systematically overestimated gap values. The electronic band structure of α-GaN calculated by Huang and Ching[24] is presented in Fig. 10. The results of Huang and Ching, Gorczyca and Christensen, and Xu and Ching are in agreement with each other, as well as with our experimental data and, thus, one can assign the three distinct

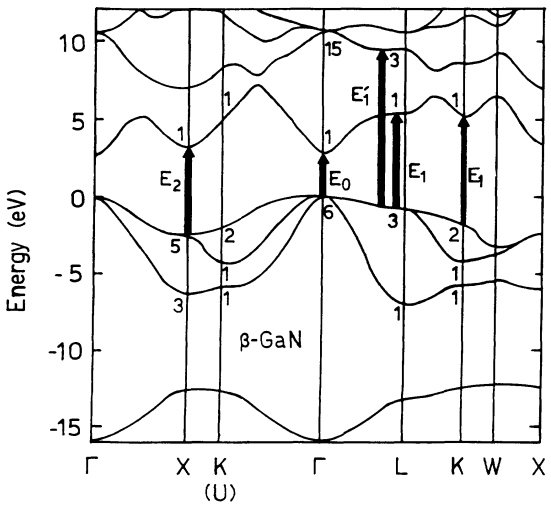

FIG. 9. Electronic band structure of cubic GaN [after Miwa and Fukumoto (Ref. 28)]. The arrows indicate the interband transitions assigned to the observed experimental structures.

structures E_{1H}, E_{2H}, and E_{3H}, which dominate the $\varepsilon(\omega)$ spectra and are centered at 7.0, 7.9, and 9.0 eV (refer to Fig. 1), to specific points in the BZ of the crystal.

The $\langle 111 \rangle$ direction of the BZ of the zinc-blende structure is mapped along the c axis (Γ-Δ-A) of the wurtzite BZ, as well as along three other directions perpendicular to c, which can be pushed by symmetry requirements down to the basal (Γ-Σ-M) or top (A-R-L) plane of the BZ. Therefore the E_1 gap, which is by definition associated with transitions in the $\langle 111 \rangle$ direction, is split in wurtzite materials into two[57] or more[56] distinct peaks for the $E \perp c$ polarization. If $E \| c$ then the E_1 gap is found to reduce to a single peak.[56,57] In view of the above, the features E_{1H} and E_{2H} of α-GaN must correspond to the E_1 gap. If our indication for an additional structure at energy $\approx$200 meV higher than E_{1H} is confirmed, then the E_{1H} structure of α-GaN must be in fact a double structure, which would imply that the E_1 gap is comprised of three features for polarization $E \perp c$, identical to what is found for CdSe.[56] In the opposite case (i.e., E_{1H} being a single structure) α-GaN would be similar to hexagonal CdS.[57]

As can be seen in Table VI, the onset of transitions at the L point (L_{24}-L_{13}) is located between the two and close to 7.3 eV, whereas the first (M_4-M_1) and second (M_4-M_3) direct gaps at the M point occur at nearby energies, between 7.0 and 7.4 eV. These three interband excitations along the M-U-L line are thought to compose the first structure (E_{1H}) in the experimental spectra. Here it should be also noted that the E_1 gap of β-GaN (denoted E_{1C} in Fig. 1), which is associated with transitions around the L point, actually coincides in energy with the E_{1H} gap of α-GaN, which may support the argument that E_{1H} is due to transitions involving primarily the L point.

The second structure (E_{2H}) may also be related to the E_1 gap and could be related to the H_3-H_3 transition, reported to take place around 8.5 eV, and possibly to an additional contribution around the M point (M_2-M_1) that covers a broad energy region, since the corresponding bands along the U and Σ directions are found to be rather flat.[22,23] This might justify the high broadening values

TABLE V. Assignment of the E_1 and E_2 CP's of the zinc-blende Ga-V compounds to specific regions in the Brillouin zone and comparison of the respective broadening parameters at 300 K determined as described in Sec. III. (exc), (2D), and (3D) indicate fitting of the dielectric-function spectra with excitonic, two-dimensional and three-dimensional line shapes, respectively.

CP	GaAs[a]	GaP[b]	GaN[c]
	Assignment of critical points		
E_1	Λ direction ΓKL plane	Λ direction ΓKL plane	Λ direction, nearer to L possibly ΓKL plane
E_2	ΓXUL plane $[E_2(P)]$ around K point $[E_2(\Sigma)]$	ΓXUL plane $[E_2(P)]$ Δ direction $[E_2(\Delta)]$ around X point	around X point possibly in the ΓXUL plane
	Broadening parameters of critical points at 300 K (in meV)		
E_1	90 (exc) 45 (2D)	100 (exc) 60 (2D)	300 (2D)
E_2	150 (2D)	70 (3D) $[E_2(\Delta)]$ 90 (3D) $[E_2(P)]$	90 (2D)

[a]Reference 65.
[b]Reference 66.
[c]This work.

calculated for this second feature (refer to Fig. 8). Finally, at energies around and above 9.0 eV transitions at the K point of the BZ are suggested to dominate. The first and second gaps (K_3-K_2 and K_2-K_2, respectively) are found to be less than 0.5 eV apart and, thus, may be responsible for the weak third feature E_{3H} at 9.0 eV that is detected in the dielectric-function spectra. The arrows in Fig. 10 designate the location of the interband transitions assigned to the observed structures.

B. Temperature dependence of the energy gaps and broadenings

As can be seen from Fig. 5, the dependence of the E_1 and E_2 gaps of β-GaN on temperature is significantly different, the former being stronger than the latter. The temperature coefficients of the energy gaps of β-GaN are compared with the corresponding results for the GaAs (Ref. 65) and GaP (Ref. 66) in Table III. The temperature coefficient of the E_1 gap at temperatures below, as well as above 300 K ($dE_1/dT = -4.5$ and -6.4×10^{-4} eV/K, respectively) is similar, within error bars, to that of the other Ga-V compounds. On the other hand, the E_2 gap exhibits a systematically smaller temperature coefficient than GaAs and GaP. In the case of α-GaN, the temperature shifts of the E_1 and E_2 features are found to be almost identical with values 5.5 and 5.4×10^{-4} eV/K, respectively, at temperatures above 300 K.

The E_1 gap exhibits broadening parameters three times greater than those of the E_2 gap (refer to Fig. 7). This is opposite to what is observed in other group-IV (Refs. 59 and 69) and III-V compounds[55,56] (see, for example, Table V) and reinforces the suggestion that the E_1 gap represents contributions from a broad wave-vector range in the BZ (refer to Fig. 9). This is further supported by the fact that only a linear fit to the broadening data is

TABLE VI. Calculated critical-point energies of the major electronic transitions up to 10 eV of α-GaN, according to the most reliable band-structure data found in the literature. The corresponding energies of the experimental dielectric-function structures are also noted.

Transition	Huang and Ching (OLCAO)[a]	Gorczyca and Christensen (LMTO-LDA)[b]	Xu and Ching (OLCAO)[c]	This work (experiment)
	Energy (eV)			
Γ_6-Γ_1	3.50	3.44	2.65	3.35
L_{24}-L_{13}	7.24	7.37	7.05	
M_4-M_1	7.05	7.03	6.7	7.0
M_4-M_3	7.3	7.4	7.25	
H_3-H_3	8.4	8.8	8.5	7.9
M_2-M_1	8.5	8.7	8.6	
K_3-K_2	9.45	9.04	8.7	9.0
K_2-K_2	9.05	9.5	9.0	

[a]Orthogonalized linear combination of atomic orbitals with LDA adjustment, Ref. 24.
[b]Linear muffin-tin orbital method, with LDA adjustment, Ref. 25.
[c]Orthogonalized linear combination of atomic orbitals without LDA adjustment, Ref. 26.

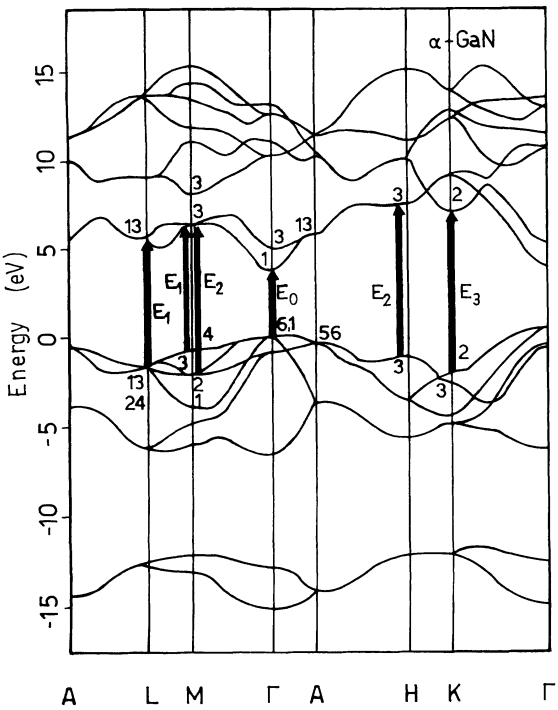

FIG. 10. Electronic band structure of hexagonal GaN [after Huang and Ching (Ref. 24)]. The arrows indicate the interband transitions assigned to the observed experimental structures.

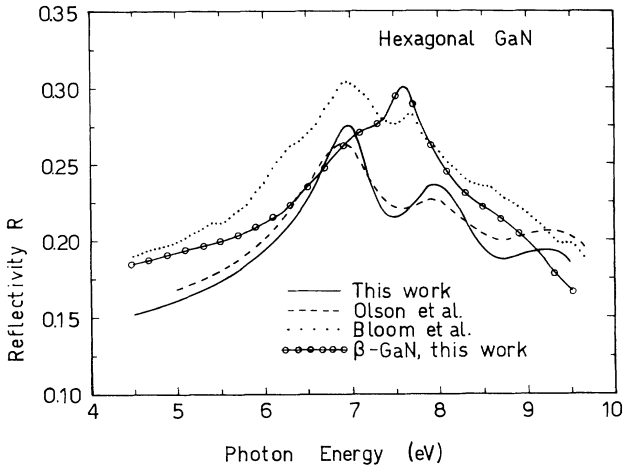

FIG. 11. The reflectivity of hexagonal GaN in the energy region 4.5–9.5 eV (solid line), deduced by ellipsometric dielectric-function measurements. The dotted and dashed lines designate the corresponding spectra presented in Refs. 23 and 47, respectively. The solid-dotted line indicates the corresponding experimental spectrum of cubic GaN.

feasible for the E_1 gap (Fig. 7), which is indicative of "inhomogeneous broadening."

C. The reflectivity of α-GaN in the energy region 4.5–9.5 eV

In all earlier works on the optical properties of hexagonal GaN the experimental technique applied was reflectivity and, therefore, it is interesting to comment on our predicted reflectivity $R(\omega)$ [as calculated from $\varepsilon_1(\omega)$ and $\varepsilon_2(\omega)$] and compare it with the data in the literature. The $R(\omega)$ spectrum of wurtzite GaN calculated in this manner in the energy region 4–10 eV is presented in Fig. 11 (solid line). The dominant features are located around 7.0 and 7.9 eV, whereas a secondary structure is evident at above 9.0 eV. The most reliable reflectivity data in the literature concern thin films with $E \perp c$ and come from Bloom *et al.*[23] and Olson, Lynch, and Zehe.[47] These spectra are shown in Fig. 11 with dotted and dashed lines, respectively. Significant discrepancies exist between these spectra concerning the line shape and the absolute values of the reflectivity.

Important differences exist concerning the absolute values of reflectivity: At the energy of 5 eV, the experimental values of reflectivity are $R = 0.17$ (Olson, Lynch and Zehe, and this work) and $R = 0.20$ (Boom *et al.*). Moreover, the absolute reflectivity value of the main peak at around 7 eV is again higher (0.30) according to Bloom *et al.* in comparison to the data of Olson, Lynch, and Zehe (0.265) and this work (0.275).

According to Fig. 11, one can see that the reflectivity maximum for α-GaN in the energy region under consideration occurs in all cases at about 7.0 eV. Two secondary peaks are noted at energies higher than the main peak at around 7.9 and above 9 eV (Olson, Lynch, and Zehe, and this work), whereas Bloom *et al.* detects three peaks in the above energy region (at 7.7, 8.6, and 9.3 eV, respectively). In order to interpret these differences we present the reflectivity spectrum of cubic GaN for comparison (solid-dotted line in Fig. 11). The higher maximum is shifted by ≈ 0.6 eV with respect to α-GaN and is located at the same energy as a peak reported by Bloom *et al.* for α-GaN. Moreover, the reflectivity line shape of Bloom *et al.* above 8 eV resembles rather that of β-GaN than that of the wurtzite modification, while the absolute values of reflectivity of β-GaN and Bloom's *et al.* data at 5 eV are in rather good agreement.

These observations may be related to one or more reasons: A possible oblique orientation of the surface plane with respect to the c axis would lead in a midcase between the $E \perp c$ and $E \| c$ polarizations[56] and, thus, nonreproducible spectral differences between them, a fact which is actually mentioned in Ref. 19. Furthermore, poor specimen quality and visible imperfections are reported to cause an uncertainty in the reflectivity peak positions of 0.1 to 0.4 eV,[23] whereas the similarities with β-GaN cannot exclude the presence of a significant cubic component in the material. We thus conclude that the reflectivity data on hexagonal GaN reported in this work are in very good agreement with those of Ref. 47, whereas other factors seem to influence the corresponding data of Ref. 23. It should be also noted that, compared to this work, the data of Ref. 47 exhibit broader features, which may be related to the specimen surface quality, a factor that greatly influences the absolute values of reflectivity at these energies.

D. The structure around 14 eV in the reflectivity spectra of α-GaN

Reliable measurements cannot be performed by our ellipsometric apparatus in the region 10–14 eV due to

second-order diffraction in the monochromator, which distorts the dielectric-function line shape and absolute values. Apart from a weak structure at around 11 eV, a broad pronounced structure at 14 eV, which is not shown in the experimental data of Fig. 13, dominates our α-GaN spectra and it is intriguing to investigate if this is an "artifact" or not. We thus consider the corresponding reflectivity spectrum of Olson, Lynch, and Zehe,[47] which exhibits both the weak feature at 11 eV and this huge feature in the region around 14 eV. Since the data extend over a wide energy range, we can directly compare the experimental dielectrical function determined by ellipsometry with the dielectric function found by Olson, Lynch, and Zehe via Kramers-Kronig analysis. The phase parameter $\theta(\omega)$ is given by the relation[70]

$$\theta(\omega_0)=\frac{\omega_0}{n}\int_0^{\infty}\frac{\ln[R(\omega)/R(\omega_0)]}{\omega_0^2-\omega^2}d\omega\ . \tag{6}$$

As seen from Eq. (6), the $\theta(\omega)$ can be accurately determined only if the values of reflectivity are known in the short- and long-wavelength regions. The behavior of $R(\omega)$ in the latter region can be well approximated by an exponential law of the form

$$R(\omega)=R(\omega_{up})(\omega_{up}/\omega)^s\ , \tag{7}$$

where ω_{up} is the upper limit of measurement. Since the upper limit of the Olson, Lynch, and Zehe data is 33 eV, which is well above the experimentally observed plasma frequency of GaN (17 eV) and sufficiently higher than the transitions from the d bands of Ga (around 22 eV), one can assume no contribution from interband transitions at energies higher than 33 eV and, therefore, consider the exponent s equal to 4 ($s=4$).[70]

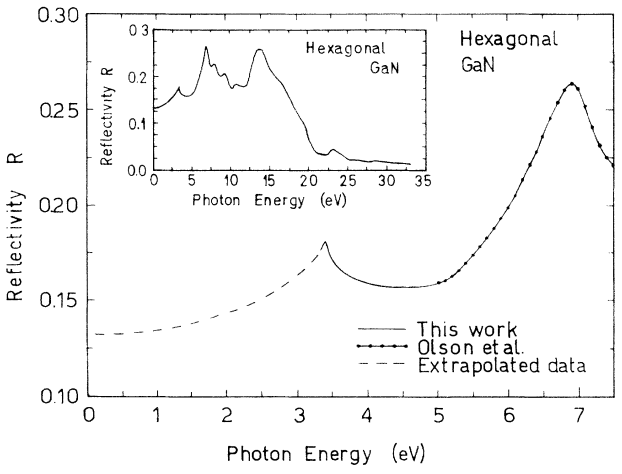

FIG. 12. The reflectivity of hexagonal GaN in the energy region between 0.05 and 7.5 eV. Solid line: experimental results from dielectric-function measurements on α-GaN films grown on sapphire. Solid-dotted line: Data reported in Ref. 47. Dashes: extrapolation of experimental data in the region of multiple reflections (1.5–3.2 eV) and in the transparent region down to 0.05 eV. In the inset is presented the resulting reflectivity spectrum of GaN, which was analyzed via the Kramers-Kronig transformation.

In the region below 5 eV, which is the lower limit of Olson, Lynch, and Zehe's data, the values of $R(\omega)$ cannot be solely approximated by a Sellmeier line shape, since the fundamental absorption of the material is located at around 3.3 eV. Therefore, Olson, Lynch, and Zehe's data (solid-dotted line in Fig. 12) were matched with our ellipsometry data of the α-GaN film grown on sapphire (solid line, Fig. 12). The data are in good agreement in the region 5–5.5 eV. The dashed line in Fig. 12 shows the extrapolation of the experimental data at energies below 3.3 eV by means of a Sellmeier line shape and in agreement with the literature.[71,72] Thus, the reflectivity spectrum that was considered in Eq. (6) for the determination of the parameter $\theta(\omega)$ ranged between 0 and 33 eV and is presented in the inset of Fig. 12.

The resulting dielectric-function spectrum calculated by Kramers-Kronig analysis of the reflectivity spectrum reported by Olson, Lynch, and Zehe and extended to zero and high energies as discussed above is represented by dashed lines in Fig. 13. In this we see that the pronounced reflectivity feature around 14 eV actually corresponds to a dielectric-function structure of ordinary magnitude and line shape. This fact provides an indication that this structure is not an artifact.

The experimental dielectric-function spectrum of α-GaN measured by ellipsometry in the region 14–25 eV is represented in the same figure (Fig. 13) by solid lines. It bears strong resemblance with the calculated one (dashed lines), such as common line shape, the location of the plasma energy (where ε_1 becomes zero) at 17 eV and the existence of broad weak features around 22 eV, which are attributed to electronic excitations from the d bands of Ga. Concerning the deviations between the experimental and calculated dielectric function in the energy region below 17 eV, a reinforcement by, e.g., 2% of the 14-eV reflectivity feature (see inset of Fig. 12) to a higher peak

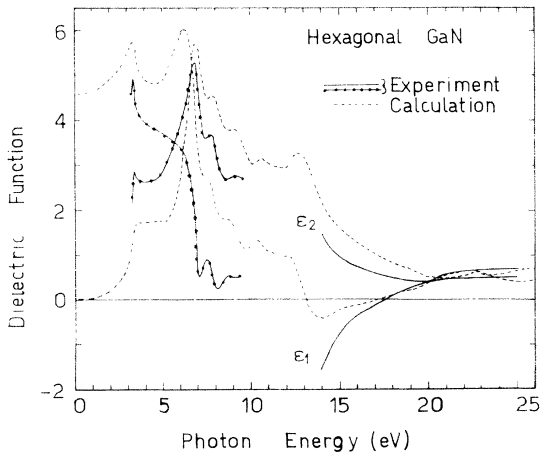

FIG. 13. The real (ε_1) and imaginary (ε_2) parts of the dielectric function of hexagonal GaN, calculated with Kramers-Kronig analysis of the reflectivity spectrum presented in the inset of Fig. 11 (dashed lines). The experimental dielectric-function spectra measured by ellipsometry in the ranges 3–9.5 and 14–25 eV are shown for comparison (solid-dotted and solid lines, respectively).

value causes the absolute values of the calculated $\varepsilon(\omega)$ to coincide with the experimental data (solid line, Fig. 13). We can also compare the calculated and the experimentally measured dielectric-function spectra of GaN in the energy region 1.5–9.5 eV. One can see that both spectra exhibit the same line shape and structures, which reinforces the conclusion that the feature reported by Olson, Lynch, and Zehe at energies around 14 eV is indeed not an artifact.

E. Average properties and sum rules in GaN

After studying the optical response of α-GaN up to 33 eV we estimate some average properties of its electronic structure, such as the ir dielectric constant ε_∞ and the effective number of valence electrons per atom n_{eff} that contribute to the optical properties. Since nitrogen forms generally bonds of short length, which affect most of the physical and optical properties of the material, a subsequent comparison between the Ga-V compounds with respect to ε_∞ and n_{eff} is of particular interest. This can be accomplished by means of the sum rules[73,74]

$$\varepsilon_\infty(\omega_m)=1+\frac{2}{\pi}\int_0^{\omega_m}\frac{\varepsilon_2(\omega)}{\omega}d\omega \tag{8}$$

and

$$n_{\text{eff}}(\omega_m)=\frac{m}{4\pi Ne^2}\frac{2}{\pi}\int_0^{\omega_m}\omega\varepsilon_2(\omega)\,d\omega\ , \tag{9}$$

where ω_m denotes the upper limit of integration. Note that Eq. (8) converges much faster than Eq. (9). The quantities m and e denote the electron mass and charge, whereas N stands for the electrons density. The volume of the α-GaN unit cell was calculated at around 45.0 A^3 from lattice parameter data.[75] Hence, in order to determine $\varepsilon_\infty(\omega_m)$ and $n_{\text{eff}}(\omega_m)$ for α-GaN from Eqs. (8)–(9) we used the calculated dielectric-function spectrum of Fig. 13.

The results for α-GaN are presented in Figs. 14 and 15, respectively, along with the corresponding ones for GaAs and GaP.[73] The corresponding results for the cubic phase, β-GaN, are estimated using the experimental spectra up to 9.5 eV and shown by the solid-dotted lines in Figs. 14 and 15.

Figure 14 provides a description of the virtual interband transitions, which are predominantly responsible for the magnitude of the dielectric constant. In the case of GaAs and GaP, the principal contribution seems to arise from transitions around and below 5 eV, whereas for GaN this region extends to around 10 eV since its major oscillator strength is located in the vacuum ultraviolet (6.5–9 eV). The asymptotic limit of the effective dielectric constant for $\omega_m\rightarrow\infty$ is found to be $\varepsilon_\infty=4.5$, somewhat lower than the direct experimental observations. The existence of the Ga d-band excitations is expected to underestimate slightly the saturation value of ε_∞ by a magnitude of less than 0.3, in comparison to dc-capacitance measurements and in a manner similar to GaAs and GaP.

The line shape of the effective number $n_{\text{eff}}(\omega)$ of valence electrons per atom of GaN is shown in Fig. 15.

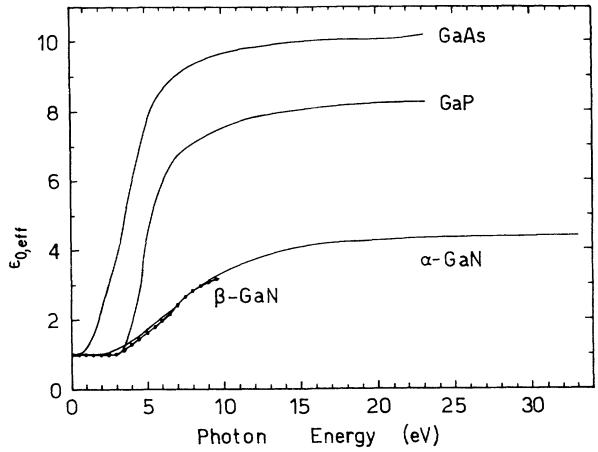

FIG. 14. The effective dielectric constant ε_∞ of α- and β-GaN vs photon energy (solid and solid-dotted lines, respectively). The corresponding data for GaP and GaAs are shown for comparison (after Ref. 73).

The $n_{\text{eff}}(\omega)$ curve of GaN exhibits higher absolute values than that of GaAs and GaP and has onset located at higher energy (5 eV), since GaN is a wide-band-gap compound with the prime oscillator strength sited at energies higher than 6.5 eV. Furthermore, as seen from Fig. 15, $n_{\text{eff}}(\omega)$ does not reach a saturation value at energy up to 34 eV. This is due to two reasons. First, at energies around 13 eV the broad reflectivity feature analyzed in Sec. V D (refer to the inset of Fig. 12) starts to contribute to n_{eff}, whereas core excitations from the d bands of Ga cause a further steep increase of n_{eff} at energies above 22 eV, contrary to what is observed in materials without d bands e.g., Si.[73]

VI. CONCLUSIONS

In this work, we report on the optical properties of zinc blende and wurtzite GaN films at energies up to 25

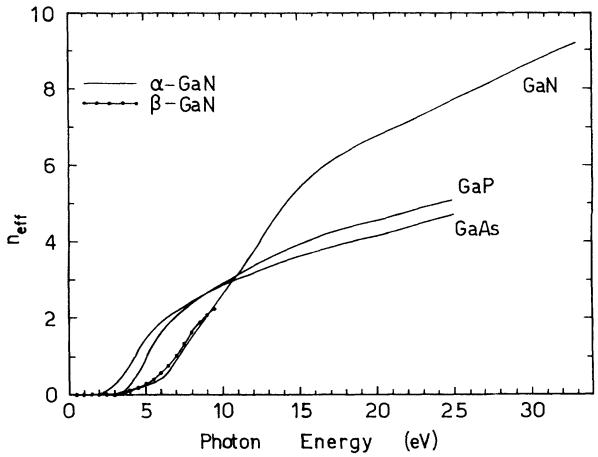

FIG. 15. The effective number of valence electrons per atom n_{eff} of α- and β-GaN vs photon energy (solid and solid-dotted lines, respectively). The corresponding data for GaP and GaAs are shown for comparison (after Ref. 73).

eV and their temperature dependence. The dielectric-function spectra of α- and β-GaN with $E \perp c$ up to 10 eV are found to bear no resemblances and exhibit different features. The fundamental gap of both polytypes is estimated to lie at different energies, namely 3.25 and 3.43 eV for the cubic and hexagonal phase.

The optical properties above the band edge are dominated in the case of β-GaN by a broad structure extending between 6.8 and 8.0 eV, which consists of at least two features. Analysis with appropriate models indicates two interband transitions, occurring at 7.0 and 7.6 eV (room temperature) and corresponding to the E_1 and E_2 gaps of the material. In conjunction with the latest electronic band-structure studies, the former CP is suggested to originate from transitions along the Λ direction, nearby the L point of the Brillouin zone, as well as from other excitations on the ΓKL plane. The high broadening values of the structure may indicate a further contribution, e.g., from an area around the K point. The E_2 structure is assigned to transitions around the X point of the Brillouin zone, but a further contribution from an extended region in the ΓXUL plane may be anticipated, in accordance to similar results for GaAs and GaP. The E_2 structure is found to be only slightly shifted with temperature, whereas E_1 shows a significantly stronger dependence. An additional structure at 8.8 eV is detected and may correspond to the E_1' gap of the material. On the other hand, the hexagonal polytype is found to exhibit three distinct peaks at 7.0, 7.9, and 9.0 eV. The first may be associated with the primary transitions at the L and M points, the second with the H_3-H_3 and M_2-M_1 excitations, whereas the third may correspond to the onset of transitions at the K point of the BZ. The features at 7.0 and 7.9 eV are thought to correspond to the E_1 gap of the material.

Furthermore, the reflectivity values of α-GaN in the region 4.5–9.5 eV estimated from the dielectric function are compared to corresponding published data and found to be in good agreement with those reported in Ref. 47, whereas a Kramers-Kronig analysis of the reflectivity is used to verify the existence of the pronounced reflectivity feature reported around 14 eV. Finally, $\varepsilon_\infty(\omega)$ and $n_{\text{eff}}(\omega)$ are calculated for α- and β-GaN at energies up to 33 eV and the results are compared between the polytypes and to those found for GaAs and GaP.

Note added in proof. We have recently become aware of a paper by Christensen and Gorczyca [Phys. Rev. B **50**, 4397 (1994)] in which a theoretical calculation of the optical response of GaN is presented.

ACKNOWLEDGMENT

This work was supported in part by the EC/LSI Program under Contract No. GE-10018-D(B).

[1]For recent reviews see, e.g., R. F. Davis, Physica B **185**, 1 (1993); S. Strite, M. E. Lin, and H. Morkoc, Thin Solid Films **231**, 197 (1993); For an older review see, F. P. Kesamanly, Fiz. Tekh Poluprovodn. B **8**, 225 (1974) [Sov. Phys. Semicond. **8**, 147 (1974)].

[2]J. S. Foresi and T. D. Moustakas, Appl. Phys. Lett. **62**, 2859 (1993).

[3]M. Asif Khan, J. N. Kuznia, D. T. Olson, J. M. Van Hove, M. Blasingame, and L. F. Reitz, Appl. Phys. Lett. **60**, 2917 (1992).

[4]I. Akasaki, H. Amano, N. Koide, M. Kotaki, and K. Manabe, Physica B **185**, 428 (1993).

[5]B. Goldenberg, J. Zook, and R. Ulmer, Appl. Phys. Lett. **62**, 381 (1993).

[6]P. Hacke, T. Detchprohm, K. Hiramatsu, and N. Sawaki, Appl. Phys. Lett. **63**, 2676 (1993).

[7]S. Nakamura, M. Senoh, and T. Mukai, Appl. Phys. Lett. **62**, 2390 (1993).

[8]K. Itoh, T. Kawamoto, H. Amano, K. Hiramatsu, and I. Akasaki, Jpn. J. Appl. Phys. **30**, 1924 (1991).

[9]M. Asif Khan, J. N. Kuznia, D. T. Olson, T. George, and W. T. Pile, Appl. Phys. Lett. **63**, 3470 (1993).

[10]Md. Rezaul Huque Khan, I. Akasaki, H. Amano, N. Okazaki, and K. Manabe, Physica B **185**, 480 (1993).

[11]A. Bykhovsky, B. Gelmont, and M. Shur, Appl. Phys. Lett. **63**, 2243 (1993).

[12]M. Asif Khan, A. Bhattarai, J. N. Kuznia, and D. T. Olson, Appl. Phys. Lett. **63**, 1214 (1993).

[13]M. Asif Khan, J. N. Kuznia, A. R. Bhattarai, and D. T. Olson, Appl. Phys. Lett. **62**, 1786 (1993).

[14]M. E. Lin, G. Xue, G. L. Zhou, J. E. Greene, and H. Morkoc, Appl. Phys. Lett. **63**, 932 (1993).

[15]T. Lei, T. D. Moustakas, R. J. Graham, Y. He, and S. J. Berkowitz, J. Appl. Phys. **71**, 4933 (1992).

[16]T. Lei, M. Fanciolli, R. J. Molnar, T. D. Moustakas, R. J. Graham, and J. Scanlon, Appl. Phys. Lett. **59**, 944 (1991).

[17]Z. Sitar, M. J. Paisley, J. Ruan, J. W. Choyke, and R. F. Davis, J. Mater. Sci. Lett. **11**, 261 (1992).

[18]M. Fanciolli, T. Lei, and T. D. Moustakas, Phys. Rev. B **48**, 15 144 (1993).

[19]E. R. Glaser, T. A. Kennedy, H. C. Crookham, J. A. Freitas, M. Asif Khan, D. T. Olson, and J. N. Kuznia, Appl. Phys. Lett. **63**, 2673 (1993).

[20]J. A. Van Vechten, Phys. Rev. **187**, 1007 (1969).

[21]D. L. Camphausen and G. A. N. Connell, J. Appl. Phys. **42**, 4438 (1971).

[22]D. Jones and A. H. Lettington, Solid State Commun. **11**, 701 (1972).

[23]S. Bloom, G. Harbeke, E. Meier, and I. B. Ortenburger, Phys. Status Solidi B **66**, 161 (1974).

[24]M-Z. Huang and W. Y. Ching, J. Phys. Chem. Solids **46**, 977 (1985).

[25]I. Gorczyca and N. E. Chistensen, Solid State Commun. **80**, 335 (1991).

[26]Y-N. Xu and W. Y. Ching, Phys. Rev. B **48**, 4335 (1993).

[27]P. Perlin, I. Gorczyca, and N. E. Christensen, Phys. Rev. B **45**, 13 307 (1992).

[28]K. Miwa and A. Fukumoto, Phys. Rev. B **48**, 7897 (1993).

[29]Lu Wenchang, Z. Kaiming, and X. Xide, J. Phys. Condens. Matter **5**, 875 (1993).

[30]M. Palummo, C. M. Bertoni, L. Reining, and F. Finocchi, Physica B **185**, 404 (1993).

[31]A. Rubio, J. Corkill, M. L. Cohen, E. L. Shirley, and S. G. Louie, Phys. Rev. B **48**, 11 810 (1993).

[32]B. J. Min, C. T. Chan, and K. M. Ho, Phys. Rev. B **45**, 1159 (1992).

[33]T. D. Moustakas, T. Lei, and R. J. Molnar, Physica B **185**, 36 (1993).
[34]C. J. Sun and M. Razeghi, Appl. Phys. Lett. **63**, 973 (1993).
[35]H. Okumura, S. Misawa, and S. Yoshida, Appl. Phys. Lett. **59**, 1058 (1991).
[36]M. E. Lin, S. Strite, A. Agarwal, A. Salvador, G. L. Zhou, N. Teraguchi, A. Rockett, and H. Morkoc, Appl. Phys. Lett. **62**, 702 (1993).
[37]M. E. Lin, B. N. Sverdlov, and H. Morkoc, Appl. Phys. Lett. **63**, 3625 (1993).
[38]J. Sumakeris, Z. Sitar, K. S. Ailey-Trent, K. L. Moore, and R. F. Davis, Thin Solid Films **225**, 244 (1993).
[39]M. Asif Khan, J. N. Kuznia, D. T. Olson, and R. Kaplan, J. Appl. Phys. **73**, 3108 (1993).
[40]M. E. Lin, N. Sverdlov, and H. Morkoc, J. Appl. Phys. **74**, 5038 (1993).
[41]J. N. Kuznia, M. Asif Khan, D. T. Olson, R. Kaplan, and J. Freitas, J. Appl. Phys. **73**, 4700 (1993).
[42]R. C. Powell, N-E. Lee, and J. E. Greene, Appl. Phys. Lett. **60**, 2505 (1992).
[43]I. Grzegory, J. Jun, St. Krukowski, M. Bockowski, and S. Porowski, Physica B **185**, 99 (1993).
[44]M. Mizuta, S. Fujieda, Y. Matsumoto, and T. Kawamura, Jpn. J. Appl. Phys. **25**, L945 (1986).
[45]B. B. Kosicki, R. J. Powell, and J. C. Burgiel, Phys. Rev. Lett. **24**, 1421 (1970).
[46]V. V. Sobolev, S. G. Kroitoru, E. B. Sokolov, and V. P. Chegnov, Fiz. Tverd. Tela (Leningrad) **20**, 3743 (1978) [Sov. Phys. Solid State **20**, 2167 (1978)].
[47]C. G. Olson, D. W. Lynch, and A. Zehe, Phys. Rev. B **24**, 4629 (1981).
[48]B. C. Chung and M. Gershenzon, J. Appl. Phys. **72**, 651 (1992).
[49]R. W. Hunt, L. Vanzetti, T. Castro, K. M. Chen, L. Sorba, P. I. Cohen, W. Gladfelter, J. M. Van Hove, J. N. Kuznia, M. Asif Khan, and A. Franciosi, Physica B **185**, 415 (1993).
[50]S. Logothetidis, J. Petalas, T. D. Moustakas, and M. Cardona, Mater. Sci. Eng. B (to be published).
[51]See, e.g., R. M. A. Azzam and H. M. Bashara, in *Ellipsometry and Polarized Light* (North-Holland, Amsterdam, 1977).
[52]M. Cardona, *Modulation Spectroscopy* (Academic, New York, 1969).
[53]J. Barth, R. L. Johnson, and M. Cardona, in *Handbook of the Optical Constants of Solids II*, edited by E. D. Palik (Academic, Orlando, 1991), p. 2193.
[54]R. L. Johnson, J. Barth, M. Cardona, D. Fuchs, and A. M. Bradshaw, Rev. Sci. Instrum. **60**, 2209 (1989).
[55]S. Logothetidis, L. Viña, and M. Cardona, Phys. Rev. B **31**, 947 (1985).
[56]S. Logothetidis, M. Cardona, P. Lautenschlager, and M. Garriga, Phys. Rev. B **34**, 2458 (1986).
[57]Ph. Hofmann, K. Horn, A. M. Bradshaw, D. Fuchs, M. Cardona, and R. L. Johnson, P hys. Rev. B **47**, 1639 (1993).
[58]Y. P. Varshni, Physica (Utrecht) **34**, 149 (1967).
[59]L. Viña, S. Logothetidis, and M. Cardona, Phys. Rev. B **30**, 1979 (1983).
[60]R. Dingle, D. D. Sell, S. E. Stokowski, and M. Ilegems, Phys. Rev. B **4**, 1211 (1971).
[61]J. R. Chelikowsky and M. L. Cohen, Phys. Rev. B **14**, 556 (1976); see, also, M. L. Cohen and J. R. Chelikowsky, in *Electronic Structure and Optical Properties of Semiconductors*, edited by M. Cardona, Springer Series in Solid-State Science Vol. 75 (Springer-Verlag, Berlin, 1988), p. 102.
[62]D. E. Aspnes and A. A. Studna, Phys. Rev. B **7**, 4605 (1973).
[63]M. Alouani, L. Brey, and N. E. Christensen, Phys. Rev. B **37**, 1167 (1988).
[64]S. C. Wang and B. M. Klein, Phys. Rev. B **24**, 3393 (1981); **24**, 3417 (1981).
[65]P. Lautenschlager, M. Garriga, S. Logothetidis, and M. Cardona, Phys. Rev. B **35**, 9174 (1987).
[66]S. Zollner, M. Garriga, J. Kircher, J. Humlíček, M. Cardona, and G. Neuhold, Phys. Rev. B **48**, 7915 (1993).
[67]S. Logothetidis, M. Alouani, M. Garriga, and M. Cardona, Phys. Rev. B **41**, 2959 (1990).
[68]S. Logothetidis, M. Cardona, M. Garriga, Phys. Rev. B **43**, 11 950 (1991).
[69]P. Lautenschlager, M. Garriga, L. Viña, and M. Cardona, Phys. Rev. B **36**, 4821 (1987).
[70]F. Wooten, in *Optical Properties of Solids* (Academic, New York, 1972).
[71]A. S. Barker and M. Ilegems, Phys. Rev. B **7**, 743 (1973).
[72]E. Ejder, Phys. Status Solidi A **6**, K39 (1971).
[73]H. Ehrenreich, in *The Optical Properties of Solids*, edited by J. Tauc (Academic, New York, 1966), pp. 146–149; H. R. Phillip and H. Ehrenreich, Phys. Rev. **129**, 1550 (1963).
[74]S. Logothetidis and G. Kiriakidis, J. Appl. Phys. **64**, 2389 (1988).
[75]O. Lagerstedt and B. Monemar, Phys. Rev. B **19**, 3064 (1979).